11B.1

INFLUENCE OF DIABATIC POTENTIAL VORTICITY ANOMALIES UPON WARM CONVEYOR BELT FLOW. PART I: 14-15 FEBRUARY 2003

Philip N. Schumacher, NOAA/NWS, Sioux Falls, SD
Joshua M. Boustead, NOAA/NWS, Valley, NE
Martin A. Baxter, Central Michigan University, Mount Pleasant, MI

1. INTRODUCTION

The impact of convection upon winter storm precipitation distribution has been a question for forecasters. Many Area Forecast Discussions (AFDs) issued by the National Weather Service contain reference to the potential for convection across the southern United States to "rob" or inhibit the flow of moisture northward. This has been used as a reason to lower snowfall amounts to the north because of expected or ongoing convection. However, there are times that snowfall does not appear to be reduced and other times where snowfall may be diminished. Overall, there is a lack of understanding of the role of convection in downstream stratiform precipitation and whether it is an overall negative or positive effect on snowfall.

One method to examine the role of convection is to use an inversion of potential vorticity. Positive potential vorticity (PV) anomalies develop below the level of maximum latent heating. While all precipitation is capable of producing a PV anomaly in the mid-troposphere, the amount of diabatic heating with convection makes it more efficient at producing long-lasting and larger PV anomalies. Anomalies associated with diabatic heating have been shown to have a significant impact upon cyclogenesis (Davis and Emmanuel 1991). Lackmann (2002) used a quasi-geostrophic potential vorticity inversion to show that a diabatically-produced PV anomaly resulted in an enhancement of the low-level jet ahead of the cold front. Similarly, Lackmann and Brennan (2006) showed that the positive PV anomaly associated with unforecast convection with the 25 January 2000 snowstorm along the East Coast resulted in an underforecast of the low-level onshore flow and a stronger surface cyclone. Finally, Mahoney and Lackmann (2007) examined the impact on downstream precipitation based upon the speed of movement of convection over the southeast United States. They found that in cases where the squall line moved slowly to the east, the precipitation downstream was enhanced, however where the squall line accelerated ahead of the cold front precipitation was decreased.

*_Corresponding Author address_: Philip N. Schumacher, National Weather Service, 26 Weather Lane, Sioux Falls, SD 57110; e-mail: phil.schumacher@noaa.gov

In all the above cases, convection had a significant impact in the moisture transport with in the warm conveyor belt by affecting the strength of the low-level jet, and the subsequent precipitation downstream. However, these cases were all associated with cold fronts in which the convection was nearly parallel to the low level jet it did not go through the convective band. Convection near the warm front, in which the major axis of the convective precipitation can be perpendicular to the low-level jet, is commonly observed with developing cold-season cyclones. Figure 1 shows one example from 8 March 2009 in which a weak snow band developed north of warm-frontal convection. This leads to the following questions:

1.) Is moisture being transported north by the low-level jet impeded by the convection?

2.) Does warm-frontal convection always decrease the amount of precipitation downstream of the convection?

3.) Does warm-frontal convection have other impacts on the location of the mid-level front and other mechanisms for lift?

4.) What is the impact of a poor forecast of convection by the model on subsequent precipitation farther north?

This paper will examine one case from 14-15 February 2003 in which significant rain with embedded convection occurred across Kansas and Missouri prior to the development of rain and snow over eastern Nebraska, southeast South Dakota, southern Minnesota and most of Iowa. Over one inch of precipitation was observed over western Iowa with much of this precipitation falling as freezing rain or snow (Fig. 2). A piecewise PV inversion was used to examine the role of diabatic PV anomalies that developed both with convection and with the stratiform precipitation. A simulation from the Weather Research Forecast (WRF-ARW) model was compared with output from the North American Regional Reanalysis (NARR). Many differences in precipitation seen between the models will be shown to be associated with the development and location of convection.

Section 2 provides an overview of the methodology and data used for this paper. Section 3 provides a brief synoptic overview of the event and examination of the mesoscale forcing for precipitation. Section 4 provides an examination of the potential vorticity distribution the mid-troposphere. The results of a piecewise PV inversion on both the WRF and NARR data are also presented and their impact on dynamic features which force precipitation. Section 5 presents concluding remarks.

2. DATA AND METHODOLOGY

A. Mesoscale model and data

In order to create a high-resolution, dynamically consistent dataset for analysis, events were simulated using Version 2.2 of the WRF-ARW (hereafter WRF), developed at NCAR. A 48-hour simulation was performed, with two-way nesting of three domains of 36-km, 12-km, and 4-km resolution. The resolution in the vertical is comprised of 50 levels, with a model top of 100 hPa. Initial and lateral boundary conditions (updated every 3 h) came from the NARR, which has a resolution of 32 km and 45 vertical layers. For convection, the Kain-Fritsch convective parameterization was used on the two outermost domains, with explicit convection on the innermost domain. Physical parameterizations chosen include the Lin et al. microphysics scheme, the YSU planetary boundary layer scheme, the Monin-Obukhov surface layer scheme, and the thermal diffusion land-surface scheme. In addition, shortwave and longwave radiation were parameterized using the Dudhia and RRTM schemes, respectively. As the available number of parameterizations increases, the choice of an optimal combination becomes increasingly difficult. The authors have used these parameterizations to simulate a number of events, and in most cases the results are sufficient for use as a proxy for the real atmosphere to conduct higher-resolution analysis of the relevant dynamics.

The precipitation output from the WRF and NARR was compared to the Cooperative Network Data administered by the National Weather Service and archived at the National Climate Data Center. Coooperative data were collected at each location once every 24 h with different locations reporting at different times of the day. Because little precipitation occurred outside the event discussed in this paper, a 3-day precipitation total was found using reports from 14-16 February 2003. These data were gridded using the Barnes analysis with the General Meteorological Package (GEMPAK).

B. Piecewise PV inversion

To quantify the impact of various PV anomalies, nonlinear, piecewise PV inversion was conducted on both WRF and NARR data, using the methodology outlined by Davis and Emanuel (1991). Piecewise PV inversion requires the specification of an appropriate reference state to quantitatively define the anomalies, thus filtering out the planetary-scale flow. Rather than use a centered time-mean approach which would be impossible in operational meteorology, we use the climatological mean flow for the time in question, in the form of the NARR mean computed over 1979-2001 for the appropriate month. Eighteen levels were used in the inversion, ranging from 1000 to 150 hPa, with an interval of 50 hPa. Potential temperature at 975 hPa and 175 hPa was used for the lower and upper boundary conditions, respectively. Lateral boundary conditions are set to zero, as the area of interest remains far from the lateral boundaries.

2. EVENT OVERVIEW

A large-scale confluent pattern existed over the eastern United States on 14 February 2003 (Fig. 3). A ridge was located over the Pacific northwest with a strong northern stream jet extending from western Canada into the eastern Great Lakes. The jet streak propagated southeast into the Great Lakes and by 1800 UTC the entrance region of the jet was located over Lake Superior. A long-wave trough was moving onto the southern California coast with a weaker jet stream downstream of the trough into western Texas. This trough quickly moved into north-central Mexico by 1800 UTC 14 Feb with the exit region of the 300 hPa jet extending into Arkansas and Oklahoma.

Arctic high pressure was associated with the upper-level ridge and jet streak over southern Canada. As the jet and ridge moved to the east the surface ridge moved southward into the northern plains. At the same time, low pressure associated with the southern stream wave moved from eastern Colorado into northern Oklahoma. A warm front extended from the low into southern Missouri. A broad 850 hPa thermal gradient across Missouri and Iowa at 0600 UTC increased in intensity through 1800 UTC as cold air moved south with the arctic high.

A comparison of the total precipitation in the NARR with observed precipitation (Fig. 2) and radar (not shown) showed that, while it underforecast the precipitation along the Iowa and Nebraska border, its general trend was qualitatively similar to observations in distribution and timing. When looking at the 6-h total precipitation from the NARR (Fig. 4), heavy rain extended from eastern Kansas into Missouri and Arkansas between 0000 UTC and 0600 UTC. During the next 6 hours, the heavy precipitation near the surface warm front slowly moved north, extending from eastern Kansas through central Missouri and into western Tennessee. A second area of precipitation was located north along the Nebraska and Iowa border into southeastern South Dakota. Between 1200 and 1800 UTC, precipitation increased in the mid-Missouri Valley with over 0.5 in. falling over southeast South Dakota. Heavy rain also continued from Texas northeastward into Tennessee. Precipitation across Missouri and Kansas decreased

with less than one-tenth of an inch observed. Between 1800 and 0000 UTC, two areas of precipitation were still evident - the first across eastern Nebraska and Iowa and the second from northeast Texas into Tennessee. Much of the precipitation over Nebraska, Iowa and South Dakota was snow or freezing rain while rain occurred over the remainder of the region. Near the surface warm front, total precipitation of one to three inches of rain was observed. Despite the heavy rainfall amounts over the southern Plains and mid-Mississippi Valley, over one inch of precipitation, falling as snow and freezing rain, fell over portions of Iowa and far eastern Nebraska.

A WRF simulation was also run of this event initializing at 1800 UTC 13 February and ending at 1800 UTC 15 February. The WRF overforecast precipitation across Kansas and Missouri with most of these areas receiving over an inch of rain (Fig. 2). Greater than 2 inches of rain was produced over eastern Kansas into southern Missouri. Meanwhile, in much of Iowa and South Dakota, precipitation was underforecast with less than 0.25 in. Instead, values over 0.5 in. were shifted southwest into eastern Nebraska. The 6-h precipitation from the WRF is shown in Figure 5. Between 0000 UTC and 0600 UTC 14 February, the WRF was similar to the NARR except it produced heavy rain over southwestern Kansas. The heavy precipitation expanded the next 6 h with much of southeast Kansas, southwest Missouri, and western Tennessee receiving over 1 in. of precipitation. Little precipitation was shown over Iowa or South Dakota. Between 1200 and 1800 UTC, the WRF continued to produce heavy rain from southern Missouri eastward into Kentucky and Tennessee. While precipitation extended across the mid-Missouri Valley, it was much lighter and farther west than what was observed. Finally between 1800 UTC and 0000 UTC, similar to observations, a large band of rain extended from northeast Texas into Kentucky. The WRF also had a band of precipitation develop from northern Kansas into northern Missouri which did not occur. The northern area of precipitation in Nebraska continued to be much lighter in the WRF and also farther west than what was observed.

The difference in the development of precipitation in the mid-Missouri Valley by the WRF and NARR was most evident after 1200 UTC. An examination of 700 hPa frontogenesis showed that an area of frontogenesis developed from southeast South Dakota into central Illinois by 1200 UTC. The frontogenesis strengthened as the precipitation intensified through 1800 UTC (Fig. 6a and b). At the same time, the symmetric stability decreased to the south of the boundary. This area of frontogenesis was coincident with the secondary maximum of precipitation that developed after 1200 UTC. However, while the WRF had an area of frontogenesis in the same area, it was much weaker (Fig. 6c and d). In addition, more intense frontogenesis extended from northern Kansas into northern Missouri by 1800 UTC. Finally, the symmetric stability across Iowa was higher than seen in the NARR while the symmetric stability across Missouri and Kansas was much lower. This implied that that frontal circulation was likely stronger across Missouri than over Iowa which resulted in the heavier precipitation in the WRF across Missouri between 1200 UTC and 1800 UTC. In fact after 1800 UTC, the WRF developed a narrow frontal band across Kansas and northern Missouri which continues after 0000 UTC (not shown). The primary reason for the difference in the precipitation distribution across the Missouri Valley was the result the difference in the 700 hPa front evolution during the morning of 14 February.

4. POTENTIAL VORTICITY ANALYSIS

The difference in the location of the 700 hPa front was either the result in differences in the upper-level evolution of the synoptic-scale wave and its impact on the mid-level wind field or mesoscale differences that resulted from the (lack of) development of internal potential vorticity anomalies. Because internal PV anomalies are the result of latent heat release associated with precipitation, the pseudo-reflectivity over the central United States was compared to the simulated radar taken from the 4-km WRF. At 0600 UTC, the WRF correctly predicted the development of an intense rainband across eastern Kansas into southern Missouri (Fig. 7a and b). However, the WRF also developed convection over south-central Kansas. This convection developed around 0100 UTC over southwest Kansas and had expanded to encompass much of south-central Kansas by 0600 UTC. As seen in Figure 5, this convection produced over 1 in. rain in 6 hours. By 1200 UTC, radar showed that precipitation had already developed in the mid-Missouri Valley while the WRF only showed scattered areas of very light precipitation. At the same time, the WRF had much heavier precipitation across Missouri with convection evident in southern Missouri whereas the radar showed precipitation had significantly decreased over Missouri (Fig. 7c and d). A similar trend was seen at 1800 UTC where observations showed moderate precipitation over the mid-Missouri Valley while the WRF had much lighter precipitation confined to eastern Nebraska (Fig 8a and b). At the same time, the WRF continued to produce rain over northern Missouri where radar showed no rain occurring. By 0000 UTC 15 February, radar observations had a band of moderate snow extending from eastern Nebraska into central Iowa and Illinois (Fig. 8c and d). This was along the 700 hPa front which intensified after 1800 UTC (not shown). At the same time, the WRF had a band of moderate precipitation from southwest Kansas in northern Missouri where the WRF continued to show the 700 hPa frontogenesis.

As a result of the development of convection, differences in the 700 hPa potential vorticity were seen by 0600 UTC (Fig. 9). Where the WRF developed convection, a small cyclonic PV anomaly can be seen over south-central Kansas by 0600 UTC. The PV anomaly is coincident with an area of large latent heat release associated with the convection within the model

(not shown). As the convection expanded and spread northeast, the PV anomaly intensified as it moved into southern Missouri by 1200 UTC. By 1800 UTC, the cyclonic PV anomaly within the WRF extended from northern Missouri into central Kentucky. Note that this was coincident with the location of the 700 hPa front which developed by 1800 UTC. For the NARR, where convection did not develop, a much weaker anomaly existed across Kansas at 0600 UTC and extended across central Missouri by 1200 UTC. By 1800 UTC, the cyclonic PV anomaly was located from southeast South Dakota into central Kentucky. The growth of the PV anomaly was much slower than the WRF. This was likely because in the NARR the latent heat release was associated with stratiform precipitation. While not shown, the cyclonic PV anomalies in both simulations extended through a large depth of the lower atmosphere.

A piecewise PV inversion was performed on the upper-level cyclonic anomalies and the internal PV anomalies. The balanced wind and height fields that resulted from these inversions at 1200 and 1800 UTC are shown in Figure 10 and 11 for the NARR and WRF, respectively. A visual inspection of the results of the upper-level cyclonic PV inversion at 700 hPa (panel b and d in both figures) showed little qualitative difference. Both inversions place the negative height anomaly in the same area with a weak trough extending northeast into northern Illinois. In contrast, significant differences were evident when inverting the internal PV anomalies. At 1200 UTC, while both models place a negative height anomaly over the western High Plains, they differed in the location of the trough that extended southeast of the cyclone center. At 1200 UTC, the effect of PV anomalies from the NARR had the trough from southeast Nebraska into western Tennessee while the WRF had the trough extend from northeast Kansas into western Tennessee. By 1800 UTC the inversion from the NARR (Fig. 10c) showed that the trough extended from South Dakota and Nebraska border into southwest Indiana. The WRF had the trough axis extending from the Kansas and Nebraska border into northern Missouri and Kentucky. The deformation was calculated from the balanced wind field (Fig. 12). Notice that by 1800 UTC, the deformation from the balanced wind field in both models was coincident with the location of the primary areas of frontogenesis shown in Figure 6. In the NARR, the deformation axis is from southeast South Dakota into southwest Indiana while the deformation in the WRF extended from eastern Nebraska into northern Missouri and southwest Indiana. Therefore, the role of the internal PV anomalies was to induce a wind field that determined where the mid-level frontogenesis would develop. In the case of the WRF, the rapid development of a diabatic PV anomaly resulted in the front developing across northern Kansas and northern Missouri. For the NARR, the weaker anomaly associated with the stratiform precipitation resulted in the 700 hPa front extending from northwest Iowa into Kentucky. The WRF's overforecast of precipitation in Missouri and Kansas produced strong PV anomalies and an associated misplacement of the 700 hPa front, the location of which was a crucial factor in the underforecast of precipitation in South Dakota and Iowa.

5. CONCLUDING REMARKS

A piecewise PV inversion was used to examine the role internal PV anomalies had on the distribution of precipitation during a central United States winter storm from 14-15 February 2003. Output from a WRF simulation was compared to the NARR. While over one inch of precipitation was observed over portions of Iowa, the WRF showed much lighter precipitation over Iowa and heavier precipitation over Kansas and Missouri.

Radar showed that the precipitation across the mid-Missouri Valley after 1200 UTC and intensified. On the other hand, precipitation over the mid-Missouri Valley was much weaker in the WRF while heavier precipitation was located over northern Missouri. The location of this precipitation was primarily determined by the development of a frontal circulation centered near 700 hPa. In both the NARR and WRF, symmetrically unstable air existed on the warm side of the front. Therefore, one reason for the difference in the location of the heavy precipitation was where the model placed the 700 hPa front. This can be related to the evolution of convection. The WRF produced convection over southwest Kansas after 0000 UTC 14 February. A diabatic PV anomaly associated with the convection advected into southern Missouri by 1200 UTC. This PV anomaly grew in size as the precipitation continued over Missouri over the next 6 hours and induced the development of a strong mid-level boundary across northern Missouri by 1800 UTC. As a result, the WRF produced a frontal band approximately 150 km too far south. And, with no front across Iowa, only light precipitation was able to develop in the mid-Missouri Valley as a result of moisture transport to the north of the internal PV anomaly. The NARR showed what really happened. A weaker PV anomaly developed with the stratiform precipitation over northern Missouri by 1200 UTC. As the stratiform precipitation spread northwest into the mid-Missouri Valley, the PV anomaly also expanded northwest. This anomaly then induced the development of a 700 hPa front across Iowa which enhanced the precipitation over the mid-Missouri Valley.

The stratiform precipitation which developed over Missouri after 0000 UTC 14 February and expanded north into Iowa and South Dakota was responsible for the development of an internal PV anomaly that extended from Iowa into southern Illinois. Rather than cutting off moisture, this initial area of precipitation in Kansas and Missouri was likely responsible for the development of the mid-level front that produced heavy snow and freezing rain over the mid-Missouri Valley. On the other hand, the convection forecasted by the WRF did not "rob" moisture from the northern stream precipitation. Instead, it induced the development of the mid-level front too far south after 1200 UTC that focused precipitation across Kansas and northern Missouri with

lighter precipitation in eastern Nebraska. In both cases, the 700 hPa front was a primary factor in the development of heavy precipitation from 1200 UTC 14 February through 0000 UTC 15 February. The difference was that the differing development of the internal PV anomalies resulted in different forecast locations for the 700 hPa front.

The results of this study showed that the role of (poorly forecast) convection. The role of convection and heavy rain associated with warm fronts on precipitation downstream (farther north) of the initial precipitation is more complex than simple robbing of moisture. As shown in Figure 13, the induced winds associated with internal PV anomalies have three affects – they can turn the low-level flow more westerly to the south of the anomaly which diverts the moisture to the east. They can turn low-level flow more easterly to the north of the anomaly which can bring moisture northwest. Finally, they can result in the development of deformation which enhances the mid-level frontogenesis. In this case, the role of the internal PV anomalies was to determine where the deformation would develop, resulting in frontogenesis, and hence where precipitation bands would develop. Determining where these internal PV anomalies will advect once they develop and anticipating their impact on the development of frontal bands is critical.

In addition to diagnosing the role of internal PV anomalies in the development of precipitation, this study showed that the use of piecewise PV inversions can help forecasters determine the reasons for model differences. The inversion of the internal PV anomalies in this case made it evident that the location of the mid-level frontal band was determined by the distribution of the diabatic PV anomalies. By tracing back the origin of the PV anomalies, forecasters could determine that the location of the frontal band would, in large part, be determined by whether convection developed over southern Kansas between 0000 UTC and 0600 UTC. Forecasters could then focus on the probability of convection developing in that area in determining where or if heavy snow would fall and the necessity of winter weather warnings. Also, knowledge of the reason for forecast differences allows forecasters to monitor the area for the development of convection. Should convection develop or not, then forecasters could issue or update snowfall amounts and appropriate warnings based upon their previous analysis of model solutions and determining which model was correct thereby providing additional lead time. Until piecewise PV inversions are available to forecasters, the application of conceptual models from this study and Part II (Boustead et al. 2009) as well as work by Brennan et al. (2008) can be used to help forecasters better understand the role of diabatic PV anomalies.

ACKNOWLEDGMENT: This research was supported by Grant Number S07-62782 provided by the Cooperative Program for Operational Meteorology, Education and Training.

REFERENCES

Boustead, J. M., P. N. Schumacher, and M. A. Baxter, 2009: Influence of diabatic potential vorticity anomalies upon warm conveyor belt flow. Part II: 4-5 January 2005. Preprints, *23rd Conference on Weather Analysis and Forecasting*, Omaha, NE, Amer. Meteor. Soc.

Brennan, M. J. and G. M. Lackmann, 2005: The influence of incipient latent heat release on the precipitation distribution of the 24-25 January 2000 U. S. east coast cyclone. *Mon. Wea. Rev.*, **133**, 1913-1937.

Brennan, M. J., K. M. Mahoney, and G. M. Lackmann, 2008: Potential vorticity (PV) thinking in operations: The utility of nonconservation. *Wea Forecasting*, **23**, 168-182.

Davis, C. and K. Emanual, 1991: Potential vorticity diagnostics of cyclogenesis. *Mon. Wea. Rev.*, **119**, 1929-1953.

Lackmann, G. M. 2002: Cold-frontal potential vorticity maxima, the low-level jet, and moisture transport in extratropical cyclones. *Mon Wea Rev.*, **130**, 59-74.

Mahoney, K. M. and G. M. Lackmann, 2006: The effect of upstream convection on downstream precipitation. *Wea. Forecasting*, **21**, 465-488.

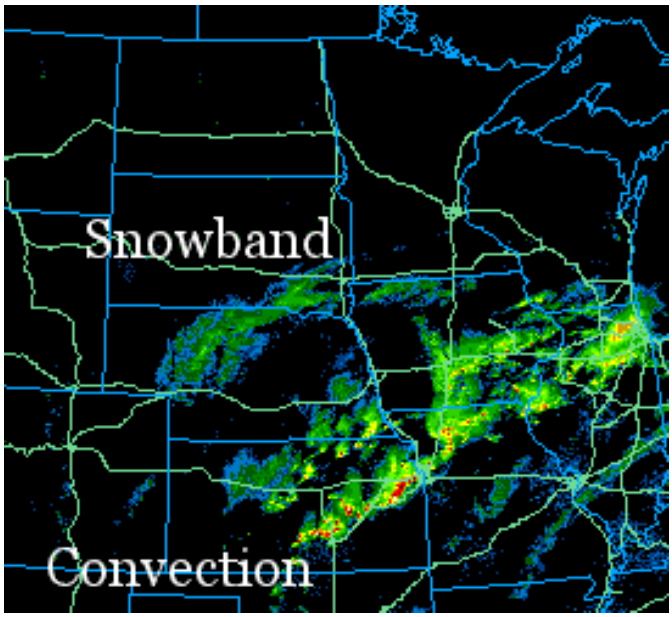

Figure 1. Mosaic radar picture from 0354 UTC 8 March 2009.

11B.1

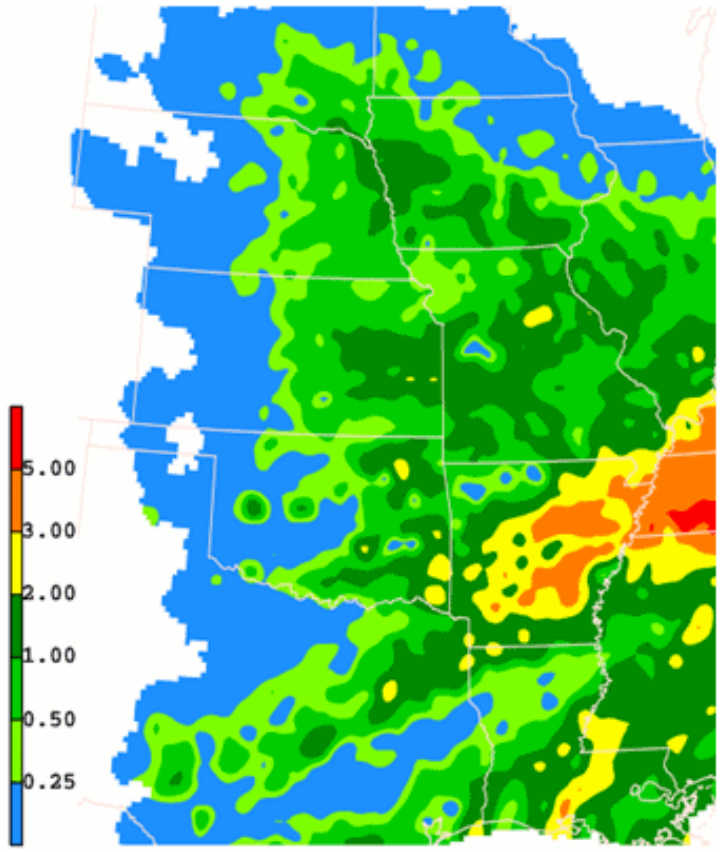

a

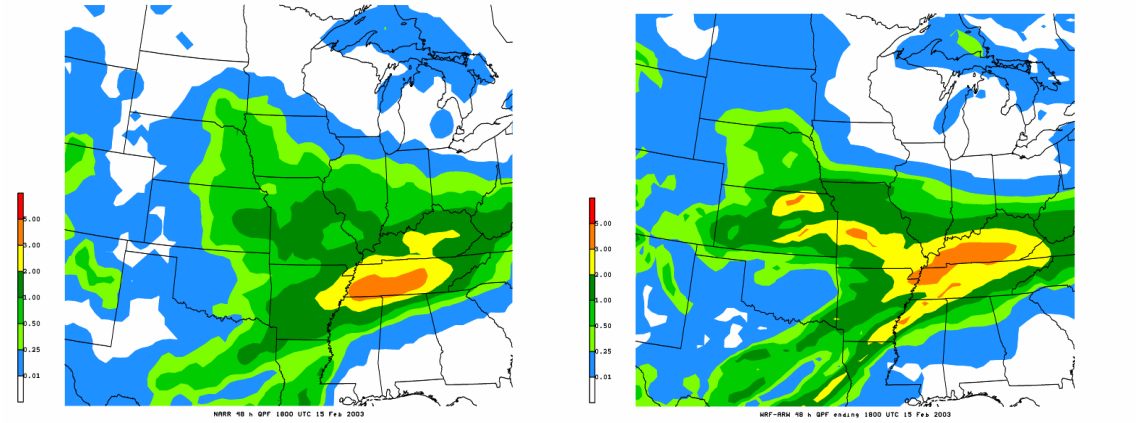

b c

Figure 2. a) Observed precipitation (in.) over the central United States from 14-16 February 2003 take from Cooperative Network data at NCDC. b) 48-h precipitation from the NARR from 1800 UTC 13 February – 1800 UTC 15 February 2003. c.) 48-h forecast precipitation from the WRF from 1800 UTC 13 February – 1800 UTC 15 February 2003.

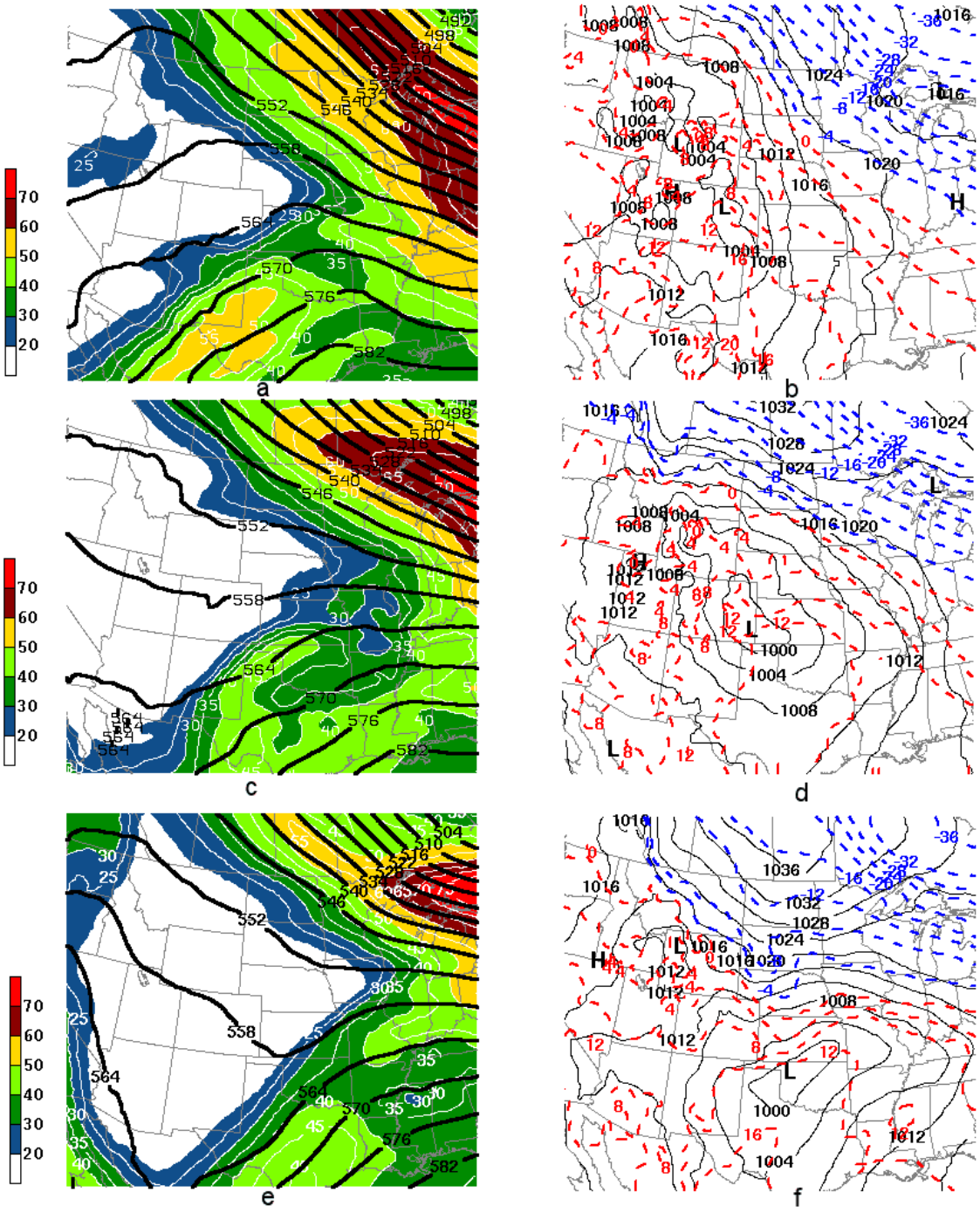

Figure 3. a, c and e) NARR depiction of the 300 hPa wind speed (m s-1, shaded and contoured every 5 m s-1) and 500 hPa height (contoured every 6 dam). b, d, and f) Mean sea level pressure (black contours every 4 hPa) and 850 hPa temperature (red (blue) dashed contours for temperature equal to or greater (less) than 0˚C, every 4˚C). Plotted times are a and b) 0000 UTC 14 February, c and d) 1200 UTC 14 February and e and f) 0000 UTC 15 February 2003.

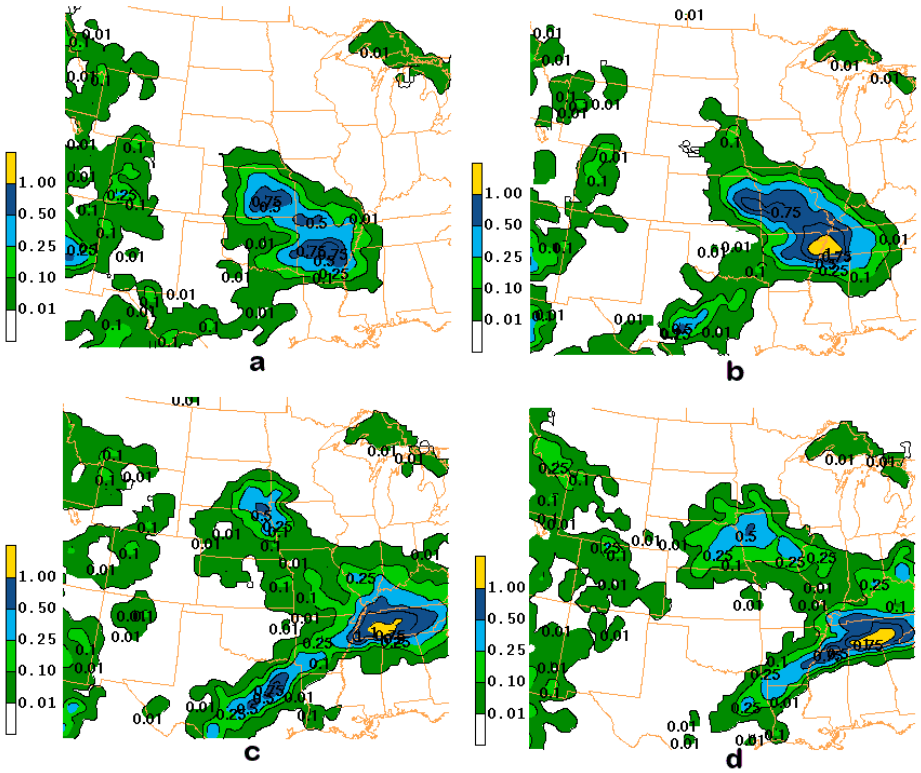

Figure 4. 6-h precipitation (in.)from the NARR ending at a) 0600 UTC 14 February, b) 1200 UTC 14 February, c) 1800 UTC 14 February, and d) 0000 UTC 15 February 2003.

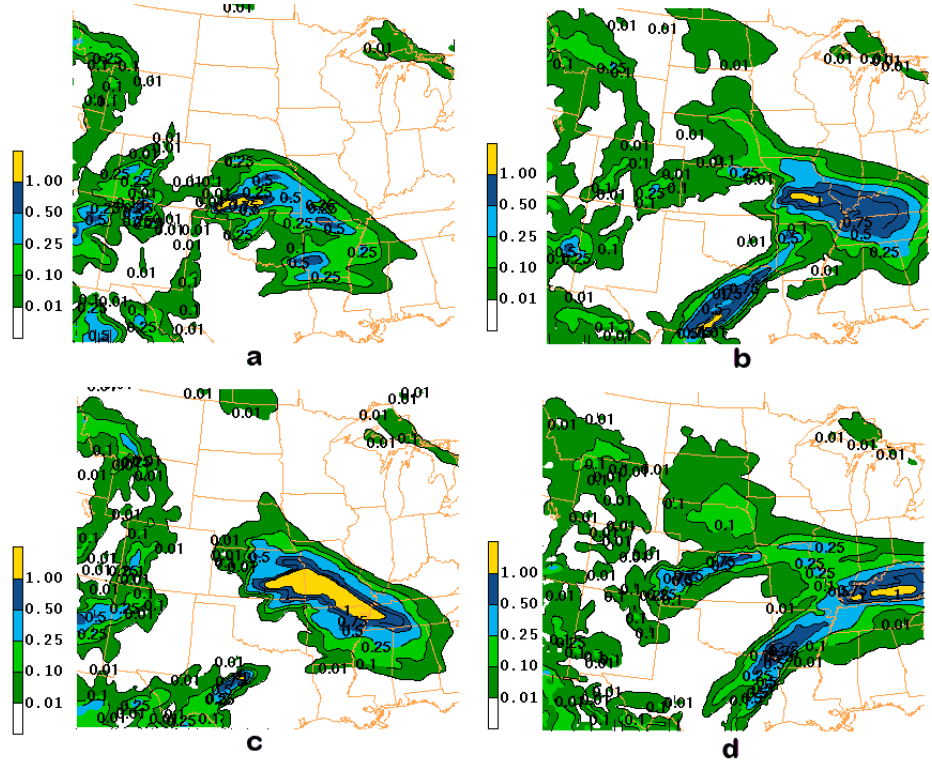

Figure 5. 6-h precipitation (in.)from the WRF ending at a) 0600 UTC 14 February, b) 1200 UTC 14 February, c) 1800 UTC 14 February, and d) 0000 UTC 15 February 2003.

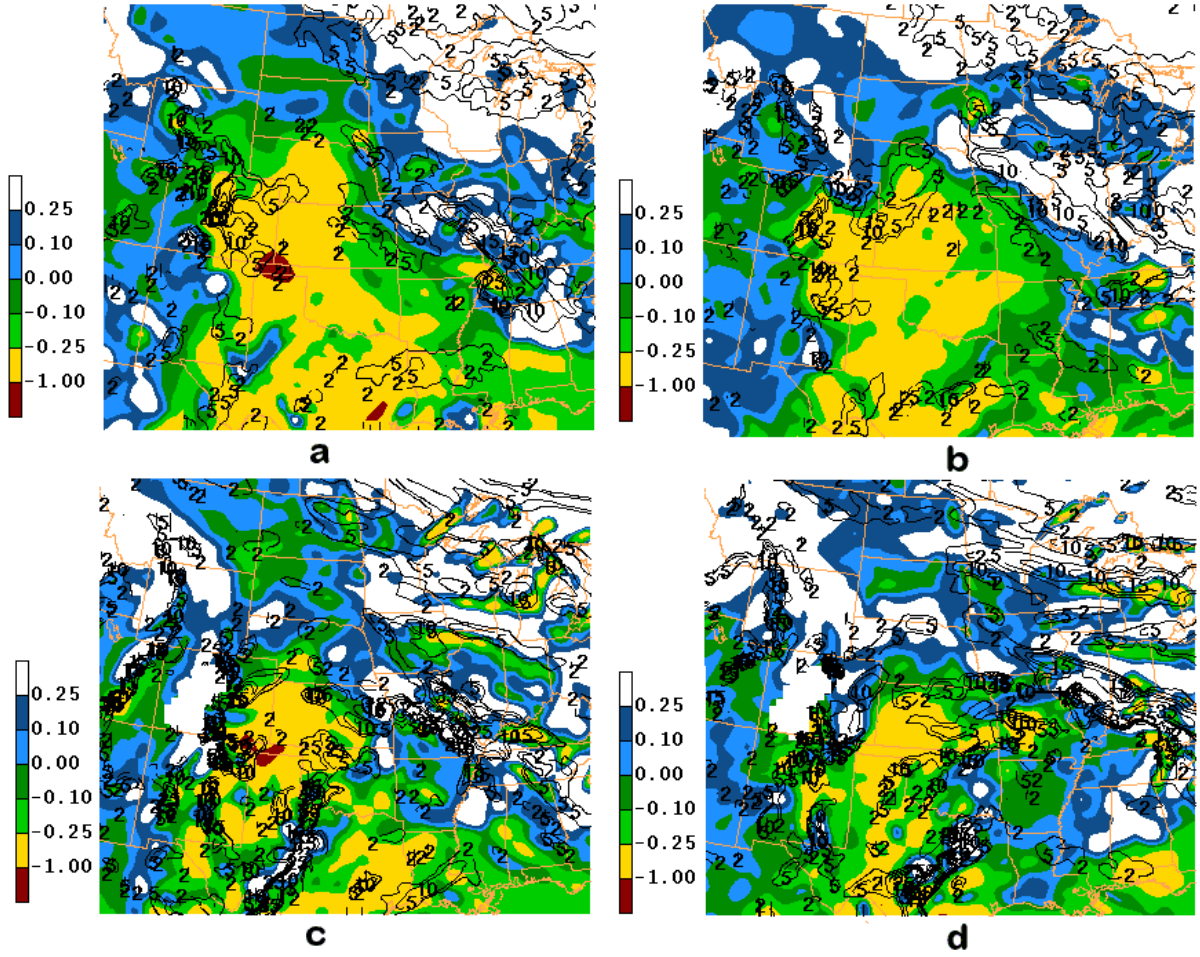

Figure 6. Frontogenesis (solid black, $x10^{1}$ ˚C (100 km)$^{-1}$ (3 h)$^{-1}$) at 700 hPa and saturated geostrophic equivalent potential vorticity (shaded < 0.25 PVU). a) NARR at 1200 UTC 14 February, b) NARR at 1800 UTC 14 February, c) WRF 18-h forecast at 1200 UTC 14 February and d) WRF 24-h forecast at 1800 UTC 14 February.

11B.1

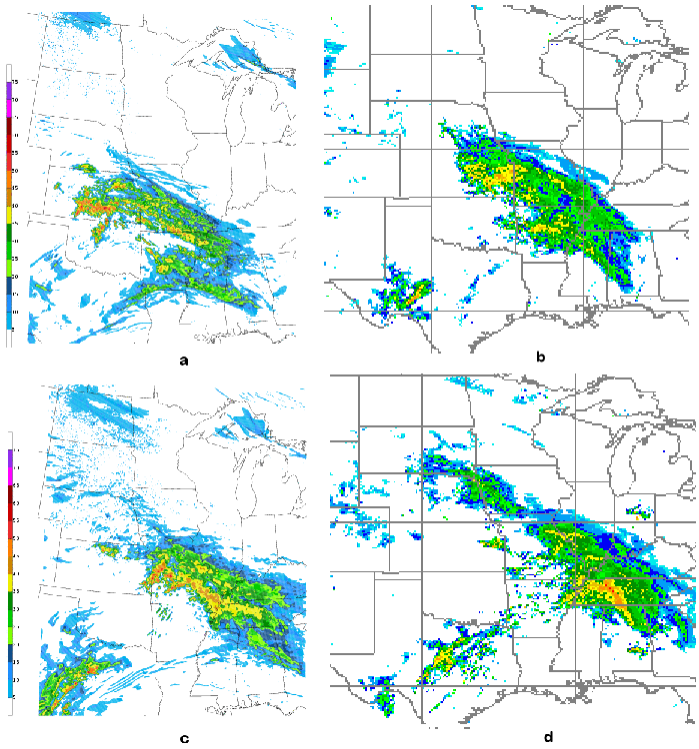

Figure 7. WRF simulated reflectivity (a and c) and radar reflectivity (b and d) from a and b) 0600 UTC 14 February and c and d) 1200 UTC 14 February.

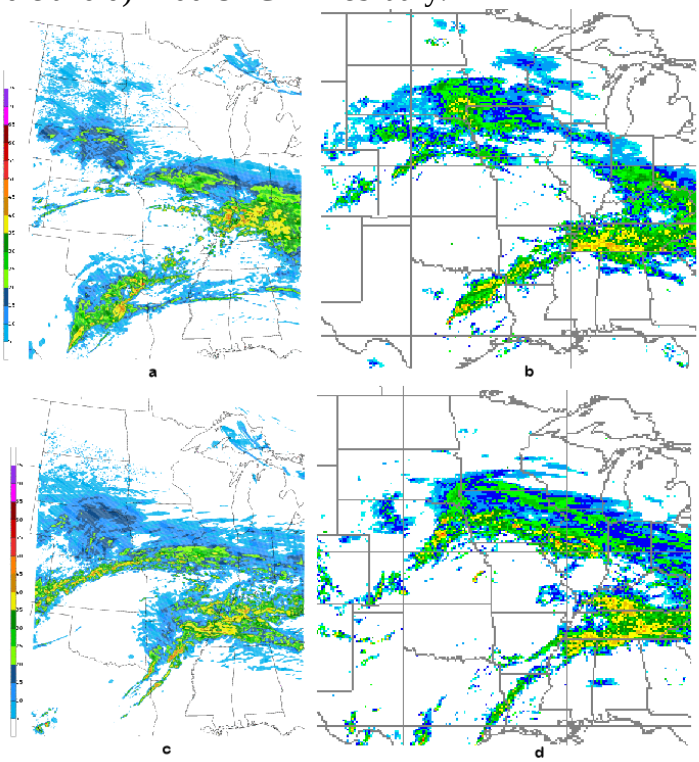

Figure 8. Same as Figure 7 except for a and b) 1800 UTC 14 February and c and d) 0000 UTC 15 February.

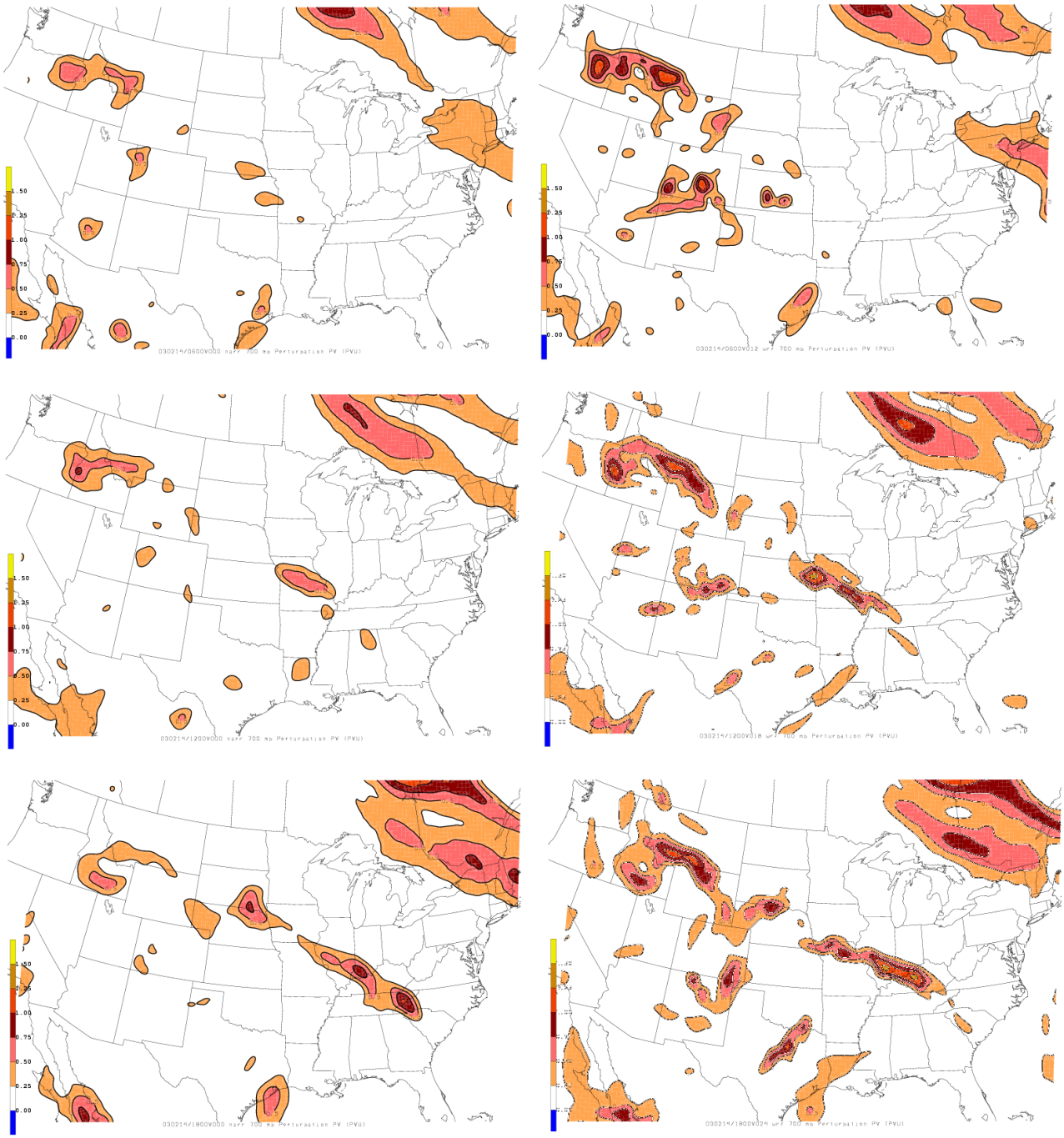

Figure 9. Cyclonic PV anomalies at 700 hPa from the NARR (a, c, and e) and WRF (b, d, and f) at a and b) 0600 UTC 14 February, c and d) 1200 UTC 14 February, and e and f) 1800 UTC 14 February 2003.

11B.1

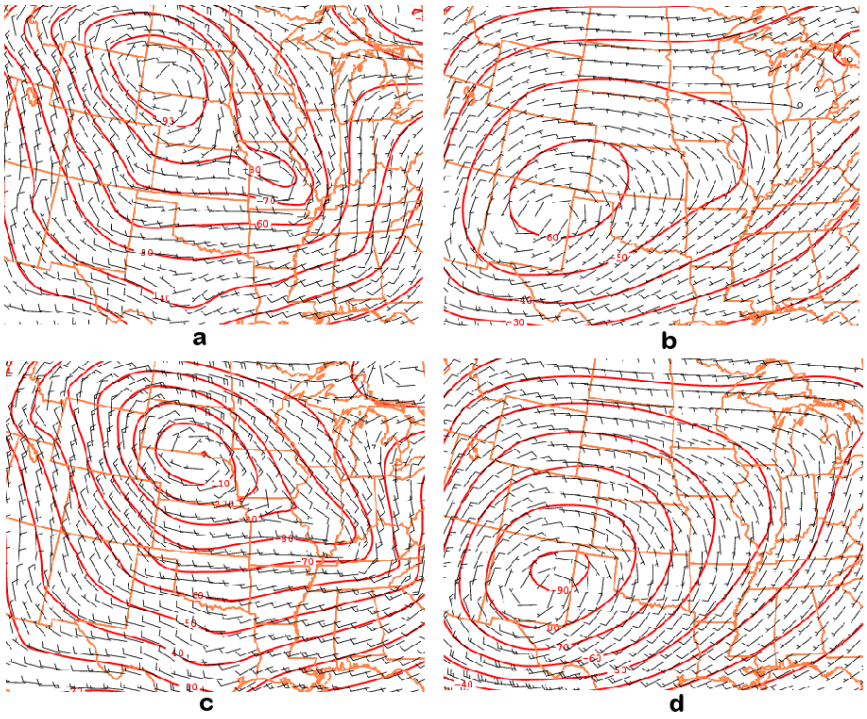

Figure 10. The 700 hPa balance wind and height fields derived from the inversion of the interior PV anomalies (a and c) and the upper-level cyclonic PV anomaly (b and d) found in the NARR. a and b) 1200 UTC 14 February 2003, c and d) 1800 UTC 14 February.

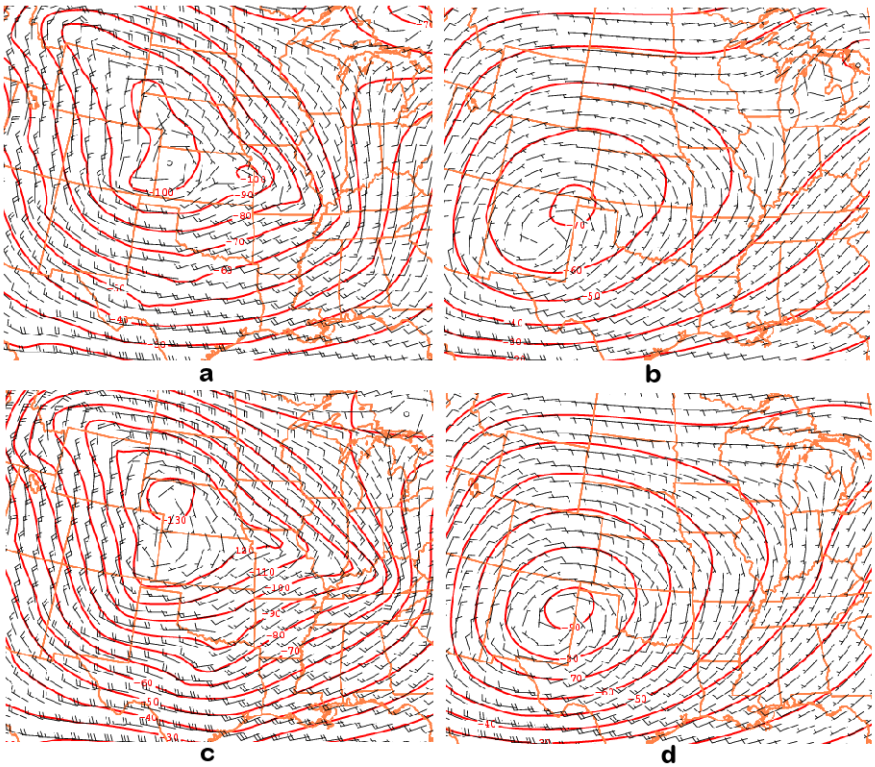

Figure 11. As in Figure 10 except for the WRF.

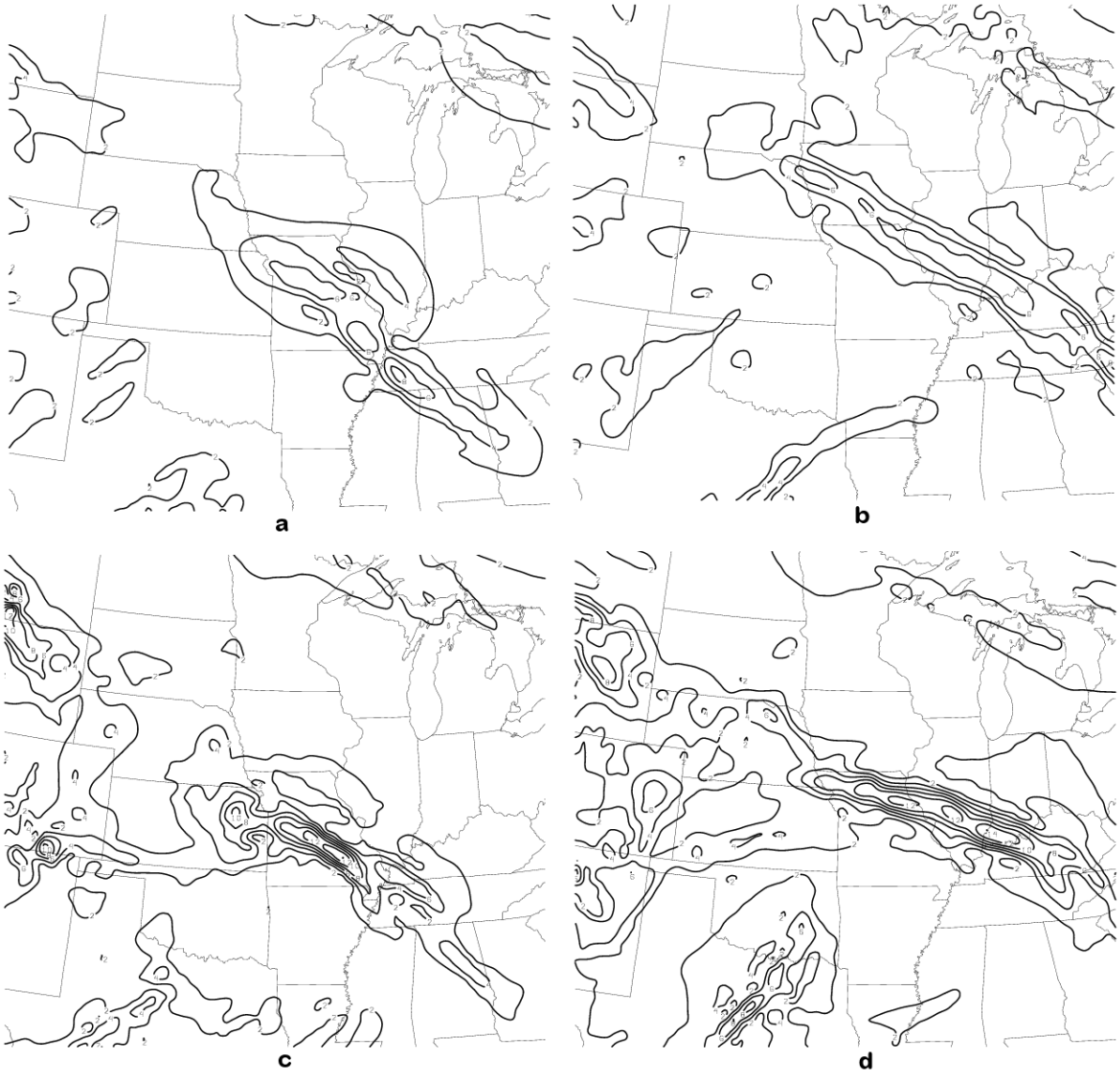

Figure 12. Resultant deformation at 700 hPa of the balanced wind field derived from the inversion of the interior PV anomalies. a) from the NARR at 1200 UTC 14 February, b) NARR at 1800 UTC 14 February, c) WRF at 1200 UTC 14 February and d) WRF at 1800 UTC 14 February.

11B.1

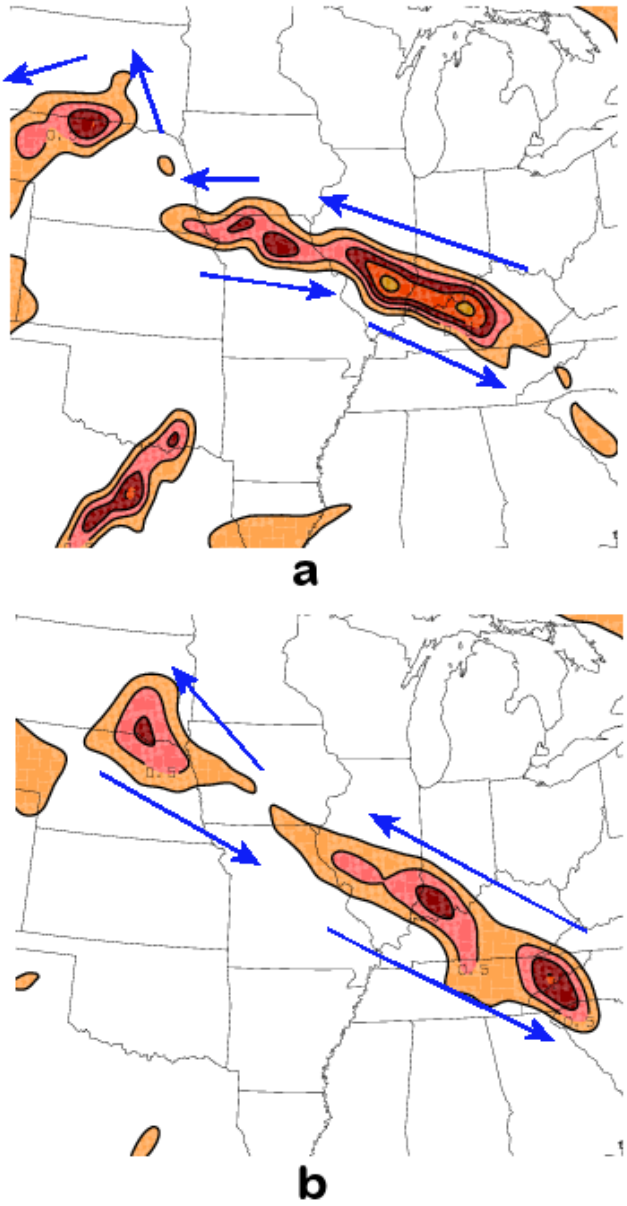

Figure 13. 700 hPa cyclonic PV anomalies at 1800 UTC 14 February from a) the WRF and b) the NARR. The blue arrows are the inferred wind circulation induced by the PV anomalies at that level.